Journal of Catalysis **212,** 22–32 (2002)
doi:10.1006/jcat.2002.3779

Enhancing the Selectivity of Benzene Hydroxylation by Tailoring the Chemical Affinity of the MCM-41 Catalyst Surface for the Reactive Molecules

He Jing, Zongying Guo, Hui Ma, David G. Evans, and Xue Duan[1]

The Key Laboratory of Science and Technology of Controllable Chemical Reactions, Ministry of Education, Beijing University of Chemical Technology, Beijing 100029, China

Received April 16, 2002; revised July 25, 2002; accepted July 31, 2002

A method of controlling selectivity to a target product in an oxidation reaction in which the target product is more reactive than the reactant is put forward in this paper. The affinity of the catalyst surface for substrates with different polarity is controlled through tailoring the surface hydrophobicity/hydrophilicity of the catalyst, thereby enhancing the selectivity. The hydroxylation of benzene is taken as the probe reaction and modified MCM-41 materials are employed as the catalysts. The catalytic performances of transition metal-substituted MCM-41, Al(III) and Ti(IV) cosubstituted MCM-41 and Ti-grafted MCM-41 materials that possess both well-ordered and long-range pore structures, indicate that the surface hydrophobicity/hydrophilicity of the catalysts does indeed significantly affect the affinity of the catalyst surface for reactant molecules with different polarity, thereby influencing the selectivity in the hydroxylation of benzene. © 2002 Elsevier Science (USA)

Key Words: **hydroxylation of benzene; chemical affinity; selectivity; MCM-41.**

1. INTRODUCTION

For the manufacture of many fine and bulk chemicals, traditional processes are environmentally unacceptable because they generally involve multistep syntheses and generate large quantities of waste products. One of the foremost challenges currently facing the chemical industry, therefore, is the need for alternative production technologies that are cleaner, safer, and more environmentally friendly. In the production of some bulk chemicals, such as acetic acid, traditional processes have largely been replaced by cleaner catalytic alternatives (1). There is currently great interest in catalytic oxidation processes for the production of fine chemicals (2). Using redox molecular sieves as catalysts, with H_2O_2 in aqueous solution as the oxidant, organic compounds such as olefins, amines, and aromatics can be transformed without the production of environmentally unfriendly side products. Most catalytic oxidation processes, including the selective oxidation of olefins and the hydroxylation of benzene, however, are potentially successive reactions, since the primary target products are more susceptible to oxidation than the reactants. As a result, the selectivity to the target product is reduced. Although the selectivity of catalysts can often be enhanced by modification of their shape selectivity, this approach is generally ineffective in such oxidation reactions. How to increase or further control the selectivity of successive oxidation reactions is still a challenge facing chemists. A method of controlling the selectivity of a successive oxidation process, named chemical affinity selectivity, is put forward in this paper. In this approach, the affinity of the catalyst surface for substrates with different polarity is controlled through tailoring the surface hydrophobicity/hydrophilicity of the catalyst, thereby enhancing the selectivity. With regard to the choice of solvent for redox reactions in which redox molecular sieves are used as catalysts, it has been suggested that the molecular sieves can be viewed as a second solvent, which extracts the substrate molecules from the bulk solvent (2). Which substrate molecules are selectively extracted is determined by the size and hydrophobicity of the pores of the molecular sieve and the substrate. Although it has been found that the surface hydrophobicity of molecular sieve catalysts influences the adsorption of substrate molecules, few reports clearly illustrate the relationship between the surface hydrophobicity/hydrophilicity and the performance of the catalyst. This paper provides preliminary experimental evidence of the feasibility of this approach. The probe reaction is taken as the hydroxylation of benzene, but this approach should be applicable to other reactions as well.

There is currently great interest in titanium-containing zeolites as catalysts for selective oxidation reactions. One disadvantage of these Ti-substituted microporous catalysts, however, is that their pore dimensions are so small as to result in diffusion resistance, especially for reactions in the liquid phase. A significant step forward has come recently

[1] To whom correspondence should be addressed. Fax: 86-10-64425385. E-mail: duanx@mail.buct.edu.cn.

0021-9517/02 $35.00

with the discovery of mesoporous silica MCM-41 (3) and the use of Ti(IV)-substituted MCM-41 as a catalyst for selective oxidation reactions (4, 5). Ti(IV)–MCM-41 offers great advantages over microporous Ti(IV)–zeolites because the active sites in Ti(IV)–MCM-41 are more accessible to the reactants.

The effects of the hydrophobicity/hydrophilicity of the catalyst surface on the catalytic performance are investigated by using transition metal-substituted, Al(III) and Ti(IV) cosubstituted, and Ti(IV)-grafted MCM-41 materials as the catalysts in this work.

2. METHODS

2.1. Chemicals and Materials

The silica gel used to prepare tetramethylammonium silicate (OH/Si = 0.26) solution and sodium silicate solution (Na/Si = 0.75) for synthesizing MCM-41 was technical grade containing 25–26 wt% silica solid. Other reagents used in this work were all A.R.

2.2. Synthesis and Characterization of Modified MCM-41 Catalysts

2.2.1. Synthesis of transition metal and/or aluminum-substituted MCM-41. Transition metal-substituted MCM-41 samples were synthesized following the literature procedure (6) using cetyltrimethylammonium bromide (CTABr) as the template. In the synthesis of Cr-, Fe-, and Ni-substituted MCM-41, an aqueous solution of $Cr(NO_3)_3$, $Fe(NO_3)_3$, or $Ni(NO_3)_2$ was added to the mixture of silicate and template. In the synthesis of Ti-substituted MCM-41, $Ti(OBu^n)_4$ was added to the mixture of silicate and template. The final gel composition was $4SiO_2 : 0.16M : CTABr : 250H_2O$ (where *M* represents Ti(IV), Cr(III), Fe(III), or Ni(II)). In the synthesis of [Si, Ti, Al]–MCM-41, an aqueous solution of $Al_2(SO_4)_3 \cdot 18H_2O$ or $NaAlO_2$ was added dropwise to the mixture after the silica source was mixed with the template solution, with Si/Al ratios of 25, 50, and 100, respectively, and with a Si/Ti ratio of 25 in the mixtures. The as-synthesized transition metal-substituted MCM-41 was calcined in air at 500°C for 10 h or longer to decompose the organic template. For chromium-substituted MCM-41, chromium(III) was introduced into the synthesis mixture but was oxidized to Cr(VI) in the calcination, as shown by the color before and after calcination (green and yellow, respectively).

2.2.2. Preparation of Ti(IV)-grafted MCM-41. Siliceous MCM-41 was synthesized following the literature procedure using cetyltrimethylammonium bromide (CTABr) as the template (7). The as-synthesized Si–MCM-41 materials were first dried in air at 100°C overnight and then calcined in air at 500°C for 10 h or longer to remove the template. The Ti(IV)-grafted MCM-41 was prepared with titanocene dichloride as the Ti(IV) source following the literature procedure (8). Varying the ratio of titanocene dichloride to MCM-41 gives Ti(IV)-grafted MCM-41 with different Ti(IV) contents, denoted as 1, 2, 3, 4, and 5% Ti-grafted samples. The as-prepared Ti(IV)-grafted MCM-41 was calcined at 500°C in air for 2 h to obtain the calcined Ti(IV)-grafted MCM-41. The color of the as-prepared Ti(IV)-grafted MCM-41 is yellow and the color of the calcined Ti(IV)-grafted MCM-41 is white.

2.2.3. Characterization. For transition metal-substituted MCM-41 materials, powder XRD patterns were obtained using an XD-D1W diffractometer with Cu $K\alpha$ radiation (40 kV, 40 mA), a step size of 0.02°, and a scan rate of 1°/min. The low-temperature N_2 adsorption–desorption experiments were carried out in a flowing system using an ST-03 adsorption instrument. The pore diameter distribution was calculated using the BJH method based on the desorption isotherm, and the surface area was calculated using the BET method based on the adsorption isotherm. Siliceous MCM-41 was also characterized on the same instruments for comparison.

For Ti(IV)-grafted MCM-41, powder XRD patterns were obtained using an XRD-6000 diffractometer with Cu $K\alpha$ radiation (40 kV, 40 mA), a step size of 0.02°, and a scan rate of 1°/min. The low-temperature N_2 adsorption–desorption experiments were carried out using a Quantachrome Autosorb-1 system. The pore diameter distribution was calculated using the BJH method based on the desorption isotherm, and the surface area was calculated using the BET method based on the adsorption isotherm. Siliceous MCM-41 for comparison was also characterized on the same instruments.

TEM micrographs were taken on a HITACHI H-800 transmission micrograph.

The XPS spectra were obtained using a VG ESCA LAB 5 spectrograph with Al $K\alpha$ radiation (9 kV, 18.5 mA). The B.E. of Ti $2p_{3/2}$ was corrected using a 103.3-eV signal of Si $2p_{3/2}$ in the same sample as the standard. The sensitivity factors used for calculation of composition were 2.04 and 0.36 for Ti and Si, respectively.

The actual metal incorporation contents were measured by the ICP technique. The ICP measurements were carried out on a ULTIMA plasma spectrometer.

The surface hydrophobicity/hydrophilicity of catalysts was evaluated by means of the temperature-programmed desorption (TPD) method. Benzene and methanol were used as the nonpolar (hydrophobic) and polar (hydrophilic) probe molecules, respectively. Benzene–TPD and methanol–TPD experiments were carried out in a custom-built TPD device using an SP3400 chromatograph as the main part and a DS 9202 data analyzer. The thermal conductivity detector was operated at 230°C. The flow rate of He carrier gas was 50 ml/min and the temperature-programmed rate was 5°C/min.

2.3. Hydroxylation of Benzene

Hydroxylation reactions were performed in a stirred round-bottom flask fitted with a water-cooled condenser as described in our previous report (9). A control experiment indicated that evaporation of benzene was minimal in such an experimental assembly and the loss of benzene can therefore be ignored in comparison with the conversion. Aqueous H_2O_2 (30%) was used as oxidant and acetone was used as solvent. After the mixture of benzene, solvent, and catalyst was heated to 65°C, a 30% H_2O_2 aqueous solution was added dropwise over the course 0.5 h (or 1.5 h for the Ti-substituted sample). Heating was continued for a further 3 h. Typically, the molar ratio of reactants was benzene : H_2O_2 : solvent = 1 : 3 : 5.7. The weight ratio of benzene to catalyst was typically 3.5 : 0.1 for metal-substituted MCM-41 and 6.06 : 0.1 for Ti-grafted MCM-41. Products were analyzed by gas chromatography with a capillary column coated with OA-1. The conversion of benzene was determined by the molar ratio of the sum of phenol and further oxidized products to the sum of benzene, phenol, and further oxidized products in the product mixture. TON (TOF) was calculated based on actual metal contents. The selectivity was determined by the molar ratio of phenol to the sum of phenol and further oxidized products in the reaction products. The other reaction products are mainly catechol and hydroquinone, all summed as further oxidized products in this work.

3. RESULTS

3.1. Structural Characteristics of MCM-41 Catalysts

3.1.1. Transition metal-substituted MCM-41 materials. Figure 1 shows the XRD patterns of Ti(IV)-, Cr(VI)-, Fe(III)-, and Ni(II)-substituted MCM-41 materials. The (100) reflections characteristic of the hexagonally ordered array of Si–MCM-41 (3) can be clearly observed, indicating that Ti(IV)-, Cr(VI)-, Fe(III)-, and Ni(II)-containing MCM-41 materials with well-ordered long-range structure were synthesized. The reflections shift to low angle after the introduction of transition metal ions. The detailed XRD parameters given in Table 1 show that not only are the d_{100} values and unit-cell parameters (a_0) of Ti(IV)-, Cr(VI)-, Fe(III)-, and Ni(II)-containing MCM-41 larger than that of siliceous MCM-41, but they also increase with an increase in the cation radius of the transition metal. The XRD data indicate that Ti(IV), Cr(VI), Fe(III), and Ni(II) cations have been inserted into the framework of MCM-41.

The N_2 adsorption–desorption isotherms of Ti(IV)-, Cr(VI)-, Fe(III)-, and Ni(II)-substituted MCM-41 materials are all typical of type IV, as reported for siliceous MCM-41 (3). The pore structural parameters calculated from the N_2 adsorption isotherms are given in Table 2. The data show that all Ti(IV)-, Cr(VI)-, Fe(III)-, and Ni(II)-substituted MCM-41 samples possess a unimodal pore size distribution, with pore diameters of at least 3.3 nm at the maximum, and have surface areas higher than 690 m^2/g. The distribution range of pore diameters increases with increasing cation radius of the transition metal, however, indicating that larger cations have an adverse effect on the long-range structural ordering of the materials. In the TEM micrographs shown in Fig. 2, the expected one-dimensionally ordered channels are clearly observed for the transition metal-substituted MCM-41 materials.

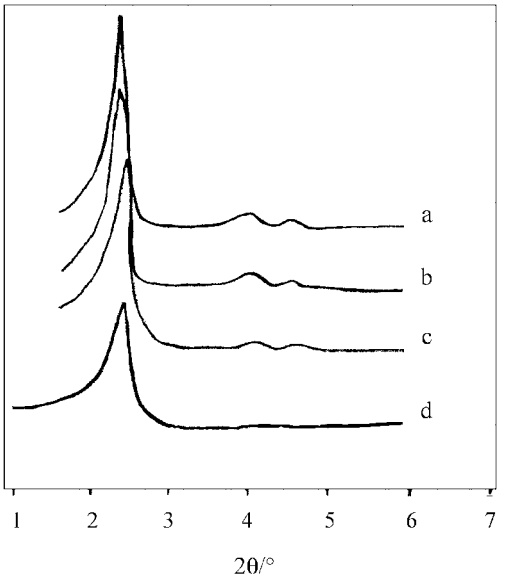

FIG. 1. XRD patterns of transition metal-substituted MCM-41 materials. (a) [Si,Ni(II)]–MCM-41; (b) [Si,Cr(VI)]–MCM-41; (c) [Si,Fe(III)]–MCM-41; (d) [Si,Ti(IV)]–MCM-41.

The results from XRD, TEM, and nitrogen adsorption–desorption isotherms all clearly show that the Ti(IV)-, Cr(VI)-, Fe(III)-, and Ni(II)-containing MCM-41 materials synthesized in this work are characterized by a regular hexagonal array of one-dimensional channels and high surface areas.

TABLE 1

Relationship between Transition Metal Cation Radius and XRD Parameters for Transition Metal-Substituted MCM-41 Materials[a]

Transition metal[c]	Actual metal incorporation (wt%)	Cation radius (nm)[b]	2θ (°)	d_{100} (nm)	a_0 (nm)
—	0	0.041[c]	2.53	3.52	4.06
Cr^{6+}	5.0	0.052	2.42	3.66	4.23
Ni^{2+}	2.3	0.062	2.40	3.67	4.24
Fe^{3+}	5.5	0.064	2.39	3.69	4.26
Ti^{4+}	2.8	0.068	2.35	3.76	4.34

[a] All the Si/M ratios in the synthesis mixture are 25.
[b] Pauling radius for tetrahedral coordination.
[c] Radius of Si^{4+}.

TABLE 2

Pore Structural Parameters of Transition Metal-Substituted MCM-41 Materials[a]

Materials	Actual metal incorporation (wt%)	Transition metal cation radius (nm)[b]	Distribution range of pore diameter (nm)	Pore diameter at the maximum in the distribution (nm)	Specific surface area (m^2/g)
Si–MCM-41	0	—	3.10–3.60	3.32	798
[Si,Cr(VI)]–MCM-41	5.0	0.052	3.22–3.70	3.42	695
[Si,Ni(II)]–MCM-41	2.3	0.062	3.15–3.53	3.34	740
[Si,Fe(III)]–MCM-41	5.5	0.064	2.66–4.00	3.33	712
[Si,Ti(IV)]–MCM-41	2.8	0.068	2.60–4.44	3.52	708

[a] All the Si/M ratios in the synthesis mixture are 25.
[b] Pauling radius for tetrahedral coordination.

3.1.2. Al(III) and Ti(IV) cosubstituted MCM-41. When Al(III) is inserted into the framework of [Si,Ti(IV)]–MCM-41, the resulting [Si,Ti(IV), Al(III)]–MCM-41 exhibits much better resolved XRD reflections than does [Si,Ti(IV)]–MCM-41 itself. The XRD peaks for [Si,Ti(IV), Al(III)]–MCM-41 become less intense with decreasing Si/Al molar ratio, as reported (10) for [Si,Al(III)]–MCM-41.

The N_2 adsorption–desorption isotherms of [Si,Ti(IV), Al(III)]–MCM-41 are all typical of type IV, similar to [Si,Ti(IV)]–MCM-41. The pore structure parameters calculated from the N_2 adsorption–desorption isotherms indicate that [Si,Ti(IV),Al(III)]–MCM-41 samples possess unimodal pore size distributions, with pore diameters of at least 2.7 nm at the maximum and surface areas higher than 500 m^2/g. The pore diameters and specific surface areas decrease after the introduction of Al(III), possibly resulting from the presence of nonframework Al(III) species (9). The distribution range of pore diameters becomes narrower with increasing Al(III) content, however, indicating that the insertion of Al(III) favors the formation of a well-ordered structure, consistent with the XRD results.

The results clearly show that the [Si,Ti(IV),Al(III)]–MCM-41 materials synthesized in this work also have an ordered structure characteristic of a regular hexagonal array.

3.1.3. Ti(IV)-grafted MCM-41. Figure 3 shows the XRD pattern of as-prepared Ti(IV)-grafted MCM-41. The XRD pattern of siliceous MCM-41 is also shown for comparison. The XRD pattern is characteristic of a hexagonal array, similar to siliceous MCM-41, indicating that the

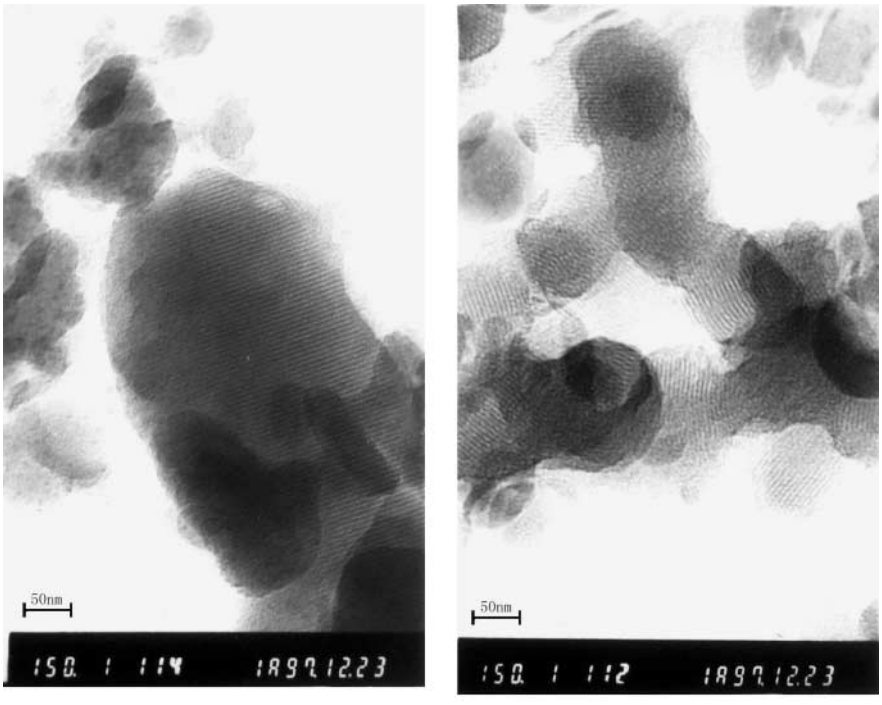

(a) [Si,Cr(VI)]-MCM-41 (b) [Si,Ti(IV)]-MCM-41

FIG. 2. TEM micrographs of transition metal-substituted MCM-41 materials.

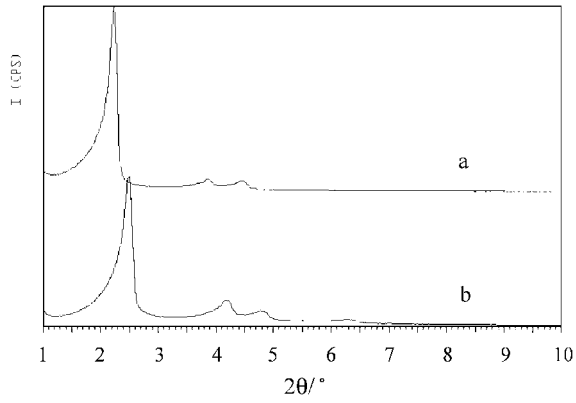

FIG. 3. XRD patterns of (a) 4% Ti(IV)-grafted MCM-41 and (b) siliceous MCM-41.

Ti(IV)-grafted MCM-41 exhibits a well-ordered long-range structure. The one-dimensionally ordered channels can also be clearly observed in the TEM micrograph shown in Fig. 4.

The N_2 adsorption–desorption isotherms of Ti(IV)-grafted MCM-41 are typical of type IV and similar to those of siliceous MCM-41. The pore size shows a narrow distribution, with a maximum at 2.39 nm. The pore structural parameters are summarized in Table 3. The grafting of Ti(IV) results in decreased pore diameter, mesopore volume, and specific surface area. The change in the pore structure parameters suggests that the titanocene moiety has been grafted onto the interior surface of MCM-41.

Figure 5 shows the XPS spectra of as-prepared Ti(IV)-grafted MCM-41. The intensity of the XPS peaks increases with increasing titanium loading (expressed as weight percent elemental Ti) in the mixture of titanocene dichloride and siliceous MCM-41. The XPS data are given in Table 4,

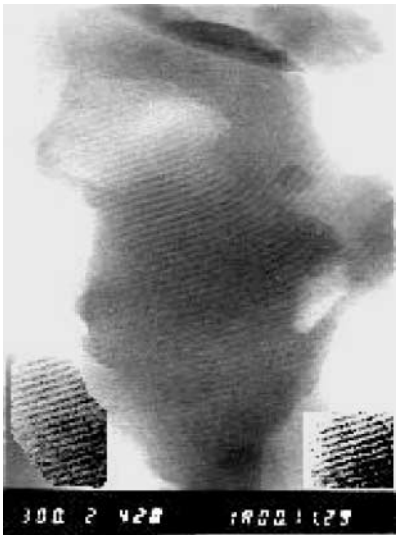

FIG. 4. TEM of 4% Ti(IV)-grafted MCM-41.

TABLE 3

Pore Structural Parameters of Ti(IV)-Grafted MCM-41 (4%) and Siliceous MCM-41

Sample	Pore diameter at the maximum in the distribution (nm)	Mesopore volume (cm^3/g)	Surface area (m^2/g)
Siliceous	2.68	0.91	1184
As prepared Ti(IV) grafted	2.39	0.71	1099
Calcined Ti(IV) grafted	2.47	0.91	1334

where it can be seen that the surface Si/Ti molar ratio gradually increases with an increase in the weight percent of Ti in the grafting mixture. The magnitude of the $2p_{3/2}$ B.E. of surface Ti(IV) decreases with an increase in the percentage of Ti, but the values are all in the range from 459.4 to 460.5eV.

Calcining the as-prepared Ti(IV)-grafted MCM-41 in air results in removal of the cyclopentadienyl rings (8), as shown in Fig. 6. The N_2 adsorption-desorption isotherms and pore size distribution profiles indicate that the calcined Ti(IV)-grafted MCM-41 possesses a pore structure similar to that of siliceous MCM-41 and the as-prepared Ti(IV)-grafted MCM-41. The pore structural parameters given in Table 3 show that the pore diameter, mesopore volume, and specific surface area all increase after calcination as a result of the removal of the cyclopentadienyl rings.

3.2. Surface Hydrophobicity/Hydrophilicity of MCM-41 Catalysts

A liquid-phase adsorption method was used to study the affinity of molecular sieves, including TS-1, [Ti(IV),Al(III)]-β, and Ti(IV)–MCM-41, for different substrates (11). In this method, partition coefficients determined from tracer liquid chromatographic experiments were used to determine in a quantitative way the organophilic or hydrophilic properties of different catalysts. An adsorption approach was also applied in defining a hydrophobicity index (HI) (12). HI is determined from the competitive gas-phase adsorption of water and a hydrocarbon on a zeolite. In this paper, the surface properties of the different MCM-41 materials were investigated by studying

TABLE 4

XPS Results of As-Prepared Ti(IV)-Grafted MCM-41 Materials

Samples	Actual Ti content (wt%)	Surface Ti/Si ratio	Ti $2p_{3/2}$ B.E. (eV)
1% Ti(IV) grafted	1.2	0.05	460.5
2% Ti(IV) grafted	1.6	0.06	460.5
3% Ti(IV) grafted	2.4	0.09	459.9
4% Ti(IV) grafted	—	0.12	459.6
5% Ti(IV) grafted	—	0.18	459.4

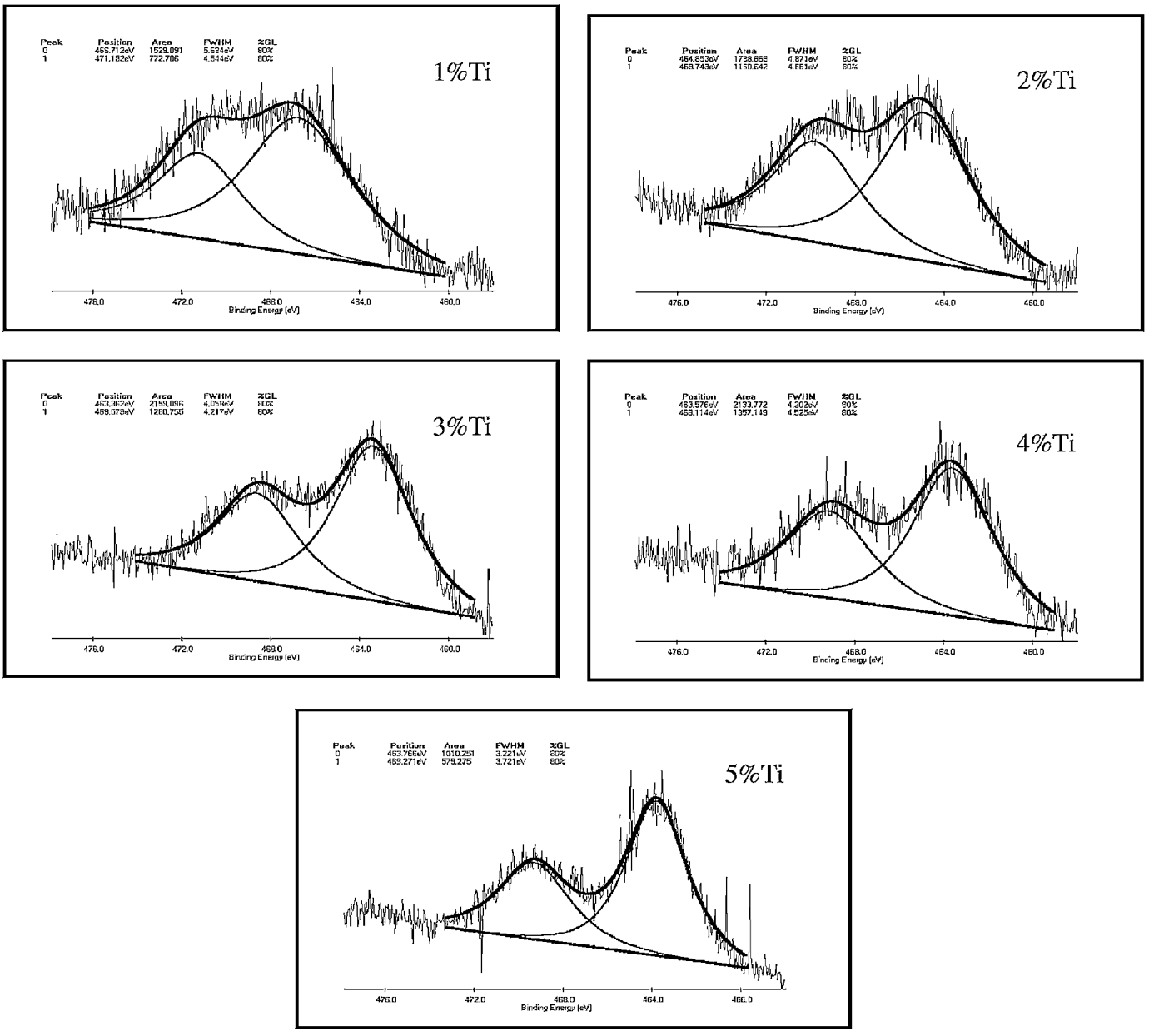

FIG. 5. XPS spectra of Ti(IV)-grafted MCM-41 with different titanocene dichloride loadings.

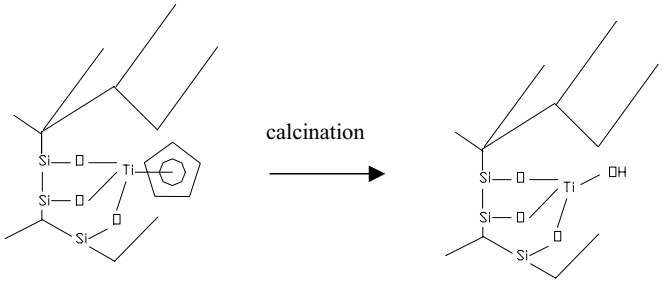

FIG. 6. Schematic model for the transformation of surface functional groups on calcination of Ti(IV)-grafted MCM-41.

the adsorption of probe molecules with different polarity. Nonpolar molecules can be expected to show affinity for hydrophobic surfaces, while, in contrast, polar molecules will show affinity for hydrophilic surfaces. The hydrophilicity/hydrophobicity of MCM-41, therefore, can be evaluated by comparison of TPD amounts of polar or nonpolar probe molecules. In this study, methanol was selected as the polar probe molecule, and benzene was chosen as the nonpolar probe molecule.

3.2.1. Transition metal-substituted MCM-41 materials. Table 5 shows the amounts of benzene and methanol desorbed from transition metal-substituted MCM-41

TABLE 5

Ratios of TPD Peak Areas of Benzene and Methanol Desorbed from Transition Metal-Substituted MCM-41

Sample	$A_{benzene}/A_{methanol}$
Si–MCM-41	218
[Si,Ti(IV)]–MCM-41	59
[Si,Cr(VI)]–MCM-41	21
[Si,Ni(II)]–MCM-41	19
[Si,Fe(III)]–MCM-41	1.1

materials in the TPD experiments. It is clear that the ratio of TPD peak areas ($A_{benzene}/A_{methanol}$) decreases dramatically following the insertion of transition metals. The change in TPD amounts of benzene and methanol indicates that the introduction of transition metals reduces the hydrophobicity but increases the hydrophilicity of the MCM-41 surface. In addition, the results in Table 5 demonstrate that the surface hydrophobicity/hydrophilicity of MCM-41 also varies with the identity of the transition metal. The hydrophobicity of transition metal-substituted MCM-41 materials decrease in the order Si–MCM-41 > [Ti(IV),Si]–MCM-41 > [Cr(VI),Si]–MCM-41 > [Ni(II),Si]–MCM-41 > [Fe(III),Si]–MCM-41. The difference in the polarity of M–O bonds (M = Ti(IV), Cr(VI), Ni(II), or Fe(III)) may be one reason for the differences in hydrophobicity/hydrophilicity of the MCM-41 surface.

3.2.2. Al(III) and Ti(IV) cosubstituted MCM-41. In order to further tailor the hydrophobicity/hydrophilicity of the MCM-41 materials, Al(III) was introduced into the Ti(IV)-modified MCM-41. Table 6 gives the TPD area ratios of benzene to methanol desorbed from [Si,Ti(IV),Al(III)]–MCM-41 with various Si/Al ratios. The insertion of Al(III) into the MCM-41 framework results in a decrease in the ratio of benzene–TPD area to methanol–TPD area. It can be concluded, therefore, that as generally expected (13), the MCM-41 surface becomes more hydrophilic and less hydrophobic with increasing Al(III) content. The TPD results for Al(III)-containing MCM-41 thus demonstrate that the TPD using probe molecules with different polarity is a feasible and reliable method for evaluating the surface hydrophilicity/hydrophobicity of solid samples.

TABLE 6

Ratios of TPD Peak Areas of Benzene and Methanol Desorbed from [Si,Ti(IV),Al(III)]–MCM-41 (Si/Ti = 25)[a]

Si/Al ratio	$A_{benzene}/A_{methanol}$
∝	59
100	33
50	26
25	15

[a] $Al_2(SO_4)_3$ as the aluminum source.

TABLE 7

Percentage Conversion of Benzene and Selectivity to Phenol for Transition Metal-Substituted MCM-41 Catalysts

Catalyst	Conversion of benzene (%)	TON (TOF)	Selectivity to phenol (%)[a]
[Si,Ti(IV)]–MCM-41	89	685 (196)	90
[Si,Cr(VI)]–MCM-41	33	142 (95)	92
[Si,Ni(II)]–MCM-41	5	47 (31)	92
[Si,Fe(III)]–MCM-41	4	16 (11)	94

[a] The other products, mainly including catechol and hydroquinone, are all summed as further oxidized products.

The above TPD results also indicate that the surface hydrophobicity/hydrophilicity of MCM-41 can be tailored through the substitution of either Al(III) or transition metals for framework silicon.

3.2.3. Ti(IV)-grafted MCM-41. For as-prepared Ti(IV)-grafted MCM-41, the titanocene moieties are anchored on the surface of the MCM-41 host through the Si–O–Ti bonding and the surface functional groups are cyclopentadiene rings, as shown in Fig. 6. The surface of the as-prepared Ti(IV)-grafted MCM-41, therefore, can be expected to be hydrophobic. But the hydrophobicity should also be expected to increase with an increase in the number of grafted titanocene moieties.

After calcination in air, the cyclopentadiene rings are removed and the surface functional groups are transformed into hydroxyl groups, as shown in Fig. 6. The surface of calcined Ti(IV)-grafted MCM-41 should be hydrophilic.

3.3. Catalytic Performance of MCM-41 Materials in Benzene Hydroxylation

3.3.1. Transition metal-substituted MCM-41 materials. Table 7 shows the percentage conversion of benzene, TON (TOF), and selectivity to phenol for transition metal-substituted MCM-41 catalysts. For comparison, the given data are the maximum values of selectivity and the respective conversions. The data show that the conversion of benzene, determined by the molar ratio of the sum of phenol and further oxidized products to the sum of benzene, phenol, and further oxidized products in the product mixture, TON (TOF), based on actual metal contents, and the selectivity to phenol, determined by the molar ratio of phenol to the sum of phenol and further oxidized products in the reaction products, all vary depending on the identity of the transition metal ion. The conversion of benzene decreases significantly in the order Ti(IV) ≫ Cr(VI) > Ni(II) ∼ Fe(III)-substituted MCM-41. The selectivity to phenol is approximately 90% in each case. The other

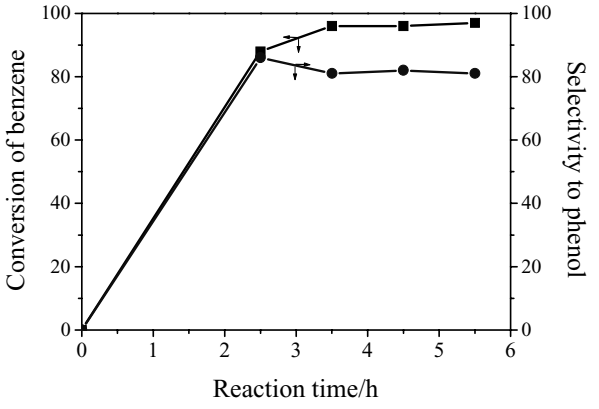

FIG. 7. Functions of the benzene conversion and selectivity to phenol as reaction time for Ti(IV)-substituted MCM-41.

reaction products are mainly catechol and hydroquinone, all summed as further oxidized products in the table.

Figure 7 shows the benzene conversion and selectivity to phenol as a function of reaction time for Ti-substituted MCM-41. The benzene conversion initially increases whereas the phenol selectivity decreases with reaction time, and then both approach constant values after 3.5 h. A total reaction time of 3.5 h is therefore sufficient for the completion of the hydroxylation reaction.

3.3.2. Al(III) and Ti(IV) cosubstituted MCM-41. Table 8 shows the percentage conversion of benzene and the phenol selectivity over [Si,Ti(IV),Al(III)]–MCM-41 (Si/Ti = 25) catalysts with different Si/Al ratios using $Al_2(SO_4)_3$ as Al source. For comparison, the conversion of benzene and the phenol selectivity over [Si,Ti(IV),Al(III)]–MCM-41 (Si/Ti = 25) catalysts (9) using $NaAlO_2$ as Al(III) source are also given. The conversion and the selectivity were determined when the reaction was complete and calculated using the same method as above. It can be observed from the data that both the conversion of benzene and the selectivity to phenol decrease significantly with decreasing Si/Al molar ratio, whether $NaAlO_2$ or $Al_2(SO_4)_3 \cdot 18H_2O$ is used as Al(III) source.

TABLE 8

Percentage Conversion of Benzene and Selectivity to Phenol for [Si,Ti(IV),Al(III)]–MCM-41 Catalysts (Si/Ti = 25 in the synthesis mixture)

	Conversion of benzene (%)		Selectivity to phenol (%)[a]	
Si/Al ratio	$Al_2(SO_4)_3$ as the aluminum source	$NaAlO_2$ as the aluminum source	$Al_2(SO_4)_3$ as the aluminum source	$NaAlO_2$ as the aluminum source
100	84	70	64	90
50	79	48	58	72
25	60	25	41	41

[a] The other products, mainly including catechol and hydroquinone, are all summed as further oxidized products.

TABLE 9

The Catalytic Performance of As-Prepared Ti(IV)-Grafted MCM-41 in the Hydroxylation of Benzene

Catalysts	Conversion of benzene (%)	Selectivity to phenol (%)[a]
1% Ti(IV) grafted	9	83
2% Ti(IV) grafted	19	84
3% Ti(IV) grafted	25	87
4% Ti(IV) grafted	87	90
5% Ti(IV) grafted	92	95

[a] The other products, mainly including catechol and hydroquinone, are all summed as further oxidized products.

3.3.3. Ti-grafted MCM-41. Tables 9 and 10 gives the percentage conversion of benzene and selectivity to phenol for as-prepared and calcined Ti(IV)-grafted MCM-41 catalysts with different Ti content, respectively. The conversion and selectivity were determined when the reaction was complete and calculated using the same method as above. The data in Table 9 show that both the conversion of benzene and the selectivity to phenol for Ti(IV)-grafted MCM-41 increase with increasing Ti content, and the selectivity to phenol is higher than 80% in each case. The data in Table 10 show that the conversion of benzene and the selectivity to phenol for calcined Ti(IV)-grafted MCM-41 exhibit no significant variation with increasing Ti content. The calcined Ti(IV)-grafted MCM-41 gives a conversion of approximately 10% in each case, lower than that observed with the as-prepared Ti(IV)-grafted MCM-41, especially in the case of high Ti content. The selectivity to phenol over calcined Ti(IV)-grafted MCM-41 is about 50% in each case, also lower than that observed with the as-prepared Ti(IV)-grafted MCM-41.

In view of the coordinatively saturated state of the Ti(IV) centers, the as-prepared Ti(IV)-grafted MCM-41 is expected to be catalytically inactive. The observed activity in the hydroxylation of benzene, however, indicates that the

TABLE 10

The Catalytic Performance of Calcined Ti(IV)-Grafted MCM-41 in the Hydroxylation of Benzene

Catalysts	Conversion of benzene (%)	Selectivity to phenol (%)[a]
1% Ti(IV) grafted	12	50
2% Ti(IV) grafted	13	45
3% Ti(IV) grafted	9	51
4% Ti(IV) grafted	10	49
5% Ti(IV) grafted	11	53

[a] The other products, mainly including catechol and hydroquinone, are all summed as further oxidized products.

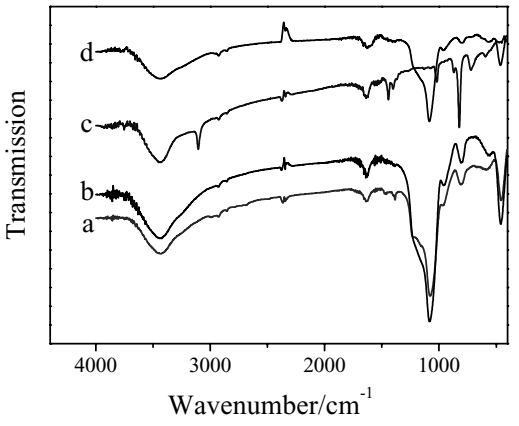

FIG. 8. FT-IR spectra of 5% Ti(IV)-grafted MCM-41: (a) as-prepared; (b) used once; (c) Cp_2TiCl_2; (d) siliceous MCM-41.

activation of H_2O_2 is possible. The reasons for the activity of as-prepared Ti(IV)-grafted MCM-41 were investigated by FT-IR and UV–vis diffuse reflectance spectra. Figure 8 shows the FT-IR spectra of Ti(IV)-grafted MCM-41. The FT-IR spectra of siliceous MCM-41 and Cp_2TiCl_2 are also shown, for comparison. In comparison with siliceous MCM-41, the as-prepared Ti(IV)-grafted MCM-41 exhibits two additional weak bands, at 1460 and 1385 cm^{-1}, which appear at 1400 and 1440 cm^{-1} for Cp_2TiCl_2. The bands at 1400 and 1440 cm^{-1} are associated with C_p rings and the coordination bonds between the C_p rings and Ti(IV) centers. After the Ti(IV)-grafted MCM-41 is used in the hydroxylation of benzene, however, the intensities of the two bands decrease very markedly, suggesting that the structure of the $C_p \rightarrow$ Ti(IV) moiety has changed. The change may result from the activation of H_2O_2. The formation of Ti(IV)–O–O–H may lead to the partial or even whole breaking of the $C_p \rightarrow$ Ti(IV) coordinate bonds. Because the IR bands are so weak, meaning some information probably could not be observed, Ti(IV)-grafted MCM-41 was studied further by diffuse reflectance UV–vis spectroscopy. As shown in Fig. 9,

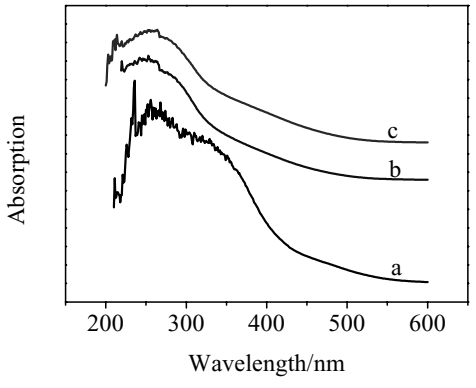

FIG. 9. UV–visible diffuse reflectance spectra of 5% Ti(IV)-grafted MCM-41: (a) as-prepared; (b) used once; (c) used twice.

the spectrum of as-prepared Ti(IV)-grafted MCM-41 exhibits a peak centered at 260 nm and a broad shoulder at 330 nm. For used Ti-grafted MCM-41, the absorption around 260 nm exhibits no obvious changes, whereas the absorption at 330 nm disappears and a shoulder at 280 nm appears. The maintenance of the major absorption at 260 nm indicates that the hydroxylation of benzene exhibits no irreversible effects on the major structure of Ti(IV) centers. Although the activation of H_2O_2 first causes a change in the coordination mode of the C_p rings from η^5- to η^3- or even η^1-, the subsequent reaction of benzene with active Ti–O–O–H leaves Ti centers coordinatively unsaturated, which allows the reforming of the η^5-$C_p \rightarrow$ Ti bonds. As a result, the structure of Ti(IV) centers is regenerated during the catalytic cycle. The presence of the shoulder at 280 nm, which is assigned to partly aggregated hexacoordinate Ti–O–Ti species or isolated TiO_x species (14–17), indicates that some Si–O–Ti bonds are broken during the hydroxylation reaction. The absorption at 330 nm for fresh Ti-grafted MCM-41 may be attributed to Ti species adsorbed on the surface, which can be leached during the hydroxylation of benzene.

4. DISCUSSION

For selective oxidation reactions using H_2O_2 or RO_2H as the oxidant, the active oxidant species may be a metal oxo or a peroxo moiety (2). Catalysis by the early transition element Ti(IV) involves a metal peroxo intermediate, whereas catalysis by other first-row transition elements, including Fe(III) or Ni(II), is believed to involve high-valence metal oxo intermediates. Cr(VI) should also involve a metal peroxo intermediate because of the vacant 3d orbits, similar to Ti(IV) species. The catalytic activity of the transition metal sites depends on the outer *d* electron density no matter which oxidant species is involved. The lower the outer *d* electron density, the stronger the capacity to activate oxidant molecules such as H_2O_2 and RO_2H. The catalytic performance of the transition metal-substituted MCM-41 materials should therefore decrease in the order Ti(IV)–MCM-41 ~ Cr(VI)–MCM-41 > Fe(III)-MCM-41 > Ni(II)–MCM-41, which deviates from the observed order Ti(IV)–Si–MCM-41 ≫ Cr(VI)–Si–MCM-41 > Ni(II)–MCM-41 ~ Fe(III)–MCM-41 (see Table 7). This indicates that some other factors may also influence the catalytic performance of transition metal-substituted MCM-41 materials. It has been demonstrated by study of the surface properties that the hydrophobicity of transition metal-substituted MCM-41 materials decreases in the order Ti(IV)–Si–MCM-41 ≫ Cr(VI)–Si–MCM-41 > Ni(II)–Si–MCM-41 > Fe(III)–Si–MCM-41 (see Table 5). The excellent catalytic performance of Ti(IV)-substituted MCM-41, therefore, may also result from its more hydrophobic surface. In the hydroxylation of benzene, as shown schematically in Fig. 10, the reactant (benzene) and intermediate

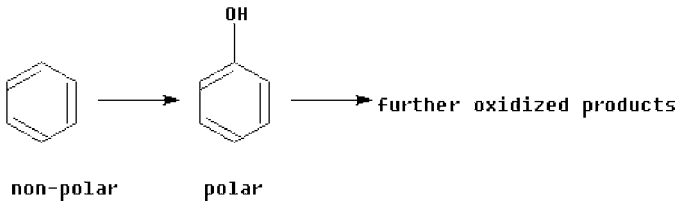

FIG. 10. Schematic representation of the hydroxylation of benzene.

target product (phenol) are very different in polarity. Benzene molecules are nonpolar, whereas phenol molecules are strongly polar. It is therefore reasonable to assume that benzene molecules will show greater affinity for hydrophobic surfaces, while in contrast, phenol molecules will show greater affinity for hydrophilic surfaces. As a result, the more hydrophobic the catalyst surface, the more readily the hydroxylation of benzene can be expected to take place, but in contrast, the more hydrophilic the catalyst surface, the more readily phenol is further oxidized to undesirable polyphenols or even tar. It can be concluded, therefore, that the high conversion of benzene and TON (TOF) of Ti(IV)-substituted MCM-41 results from both the high catalytic capacity of the Ti(IV) centers and the high affinity between the hydrophobic surface of the catalyst and nonpolar benzene. Although the observed selectivity is similar for all of the Ti(IV)-, Cr(VI)-, Fe(III)-, and Ni(II)-substituted MCM-41, the values of selectivity are measured at very different benzene conversion or TON (TOF) levels. It can be predicted, therefore, that the selectivity to phenol in Cr(VI)-, Fe(III)-, and Ni(II)-substituted MCM-41 is likely to be reduced to a great extent if the conversion of benzene or TON (TOF)approaches that in Ti-substituted MCM-41. Certainly, the observed high selectivity to phenol over each of the Ti(IV)-, Cr(VI)-, Fe(III)-, and Ni(II)-substituted MCM-41 materials is also probably related to the large pore sizes of the catalysts. For hydroxylation in the liquid phase in the presence of a solvent, the larger pores of MCM-41 allow phenol to readily diffuse away from the active sites, thus avoiding further oxidation.

The relationship between the surface hydrophobicity/hydrophilicity and the catalytic performance of [Si,Ti(IV),Al(III)]–MCM-41 further supports the above analysis of the effects of surface properties on the catalytic performance. Generally, the introduction of Al(III) can be expected to increase the hydrophilicity of zeolites (13), and also to generate either acidic or basic sites as a consequence of charge balance requirements in the framework. In our previous work (9), the catalytic performance of [Si,Ti(IV),Al(III)]–MCM-41 using $NaAlO_2$ as Al(III) source was studied and it was observed that both the conversion of benzene and the selectivity to phenol decreased with decreasing Si/Al ratios. In the case of $NaAlO_2$ as Al(III) source but not ion exchanged with H^+, introducing Al(III) most probably generates strong basic sites because of the presence of significant quantities of Na^+. These sites will adsorb phenol more strongly than benzene, since phenol is acidic and benzene is amphoteric. In addition, the presence of Na^+ increases the rate of H_2O_2 decomposition, which is possibly another reason for the reduction in benzene conversion. Thus the change in the conversion and selectivity with decreasing Si/Al ratios is not only dependent on the surface hydrophobicity/hydrophilicity of [Si,Ti(IV),Al(III)]–MCM-41 catalysts. The catalytic performance of [Si,Ti(IV),Al(III)]–MCM-41 using $Al_2(SO_4)_3 \cdot 18H_2O$ as Al(III) source has, therefore, been investigated in this paper. In the case of $Al_2(SO_4)_3 \cdot 18H_2O$ as Al(III) source, introduction of Al(III) most probably generates acidic sites and consequently increases the hydrophilicity of [Si,Ti(IV),Al(III)]–MCM-41. The higher the Al(III) content, the more hydrophilic the surface, as shown in Table 6. The variation in benzene conversion and phenol selectivity with Si/Al molar ratio indicates that the hydroxylation of benzene becomes less favorable with decreasing Si/Al molar ratios, while the hydroxylation of phenol becomes more favorable with decreasing Si/Al molar ratios of the [Si,Ti(IV),Al(III)]–MCM-41 as catalyst (Table 8). This indicates that the surface hydrophobicity/hydrophilicity of [Si,Ti(IV),Al(III)]–MCM-41 has a significant effect on the hydroxylation of aromatics with different polarity and chemical properties.

For as-prepared Ti(IV)-grafted MCM-41, the increase in benzene conversion with increasing titanium content is expected, since the number of surface Ti(IV) sites increases. The effect of surface properties on the conversion should not be neglected, however. The hydrophobicity of Ti(IV)-grafted MCM-41 is expected to increase with increasing titanocene content because grafting of titanocene transforms Si–OH groups into Si–O–TiCp moieties. As a result, the affinity of the catalyst surface for nonpolar benzene molecules increases with increasing content of surface titanocene moieties. The increase in the selectivity to phenol with increasing loading of surface titanocene moieties is also a result of the increase in the surface hydrophobicity. The enhancement of the surface hydrophobicity decreases the affinity for the polar phenol molecules, which inhibits the further oxidation of phenol. For the calcined Ti-grafted MCM-41, both the benzene conversion and the selectivity to phenol are lower than those over the as-prepared Ti(IV)-grafted MCM-41 (Tables 9 and 10). The difference between the as-prepared and calcined Ti(IV)-grafted MCM-41 in the conversion of benzene and selectivity to phenol most probably results from the differences in the surface properties. The surface of the calcined Ti(IV)-grafted MCM-41 is more hydrophilic than that of the as-prepared Ti(IV)-grafted MCM-41 (as shown in Fig. 6). As a result, the as-prepared Ti(IV)-grafted MCM-41 favors the hydroxylation of benzene whereas the calcined Ti(IV)-grafted MCM-41 favors the hydroxylation of phenol to give further oxidized products.

In conclusion, the above results indicate that catalysts with different surface hydrophobicity/hydrophilicity can show significantly different affinities for molecules with different polarity, thereby affecting the selectivity of reaction. This concept, which we suggest be called chemical affinity selectivity, is expected to be applicable to other related oxidation systems.

5. CONCLUSIONS

The selectivity in the benzene hydroxylation reaction can be improved through tailoring the chemical affinity between the catalyst surface and the reactant molecules. The chemical affinity can be controlled by tailoring the surface properties of the catalysts.

ACKNOWLEDGMENTS

The authors are grateful for financial support from the State Key Basic Research Project of China (Grant 2000 048 009) and the NSFC (Grant 20173003).

REFERENCES

1. Sheldon, R. A., *J. Mol. Catal. A* **107**, 75 (1996).
2. Arends, I. W. C. E., Sheldon, R. A., Wallau, M., and Schuchardt, U., *Angew. Chem. Int. Ed. Engl.* **36**, 1144 (1997).
3. Kresge, C. T., Leonowicz, M. E., Roth, W. J., Vartuli, J. C., and Beck, J. S., *Nature* **359**, 710 (1992).
4. Tanev, P. T., Chibwe, M., and Pinnavaia, T. J., *Nature* **368**, 321 (1994).
5. Corma, A., Navarro, M. T., and Perez-Pariente, J., *J. Chem. Soc. Chem. Commun.* 147 (1994).
6. Xu, W. P., Jing, H., Sun, P., and Duan, X., *Chem. J. Chin. Univ.* **20**, 1429 (1999).
7. Jing, H., Li, X. F., Evans, D. G., Duan, X., and Li, C. Y., *J. Mol. Catal. B* **11**, 45 (2000).
8. Maschmeyer, T., Rey, F., Sankar, G., and Thomas, J. M., *Nature* **378**, 159 (1995).
9. Jing, H., Xu, W. P., Evans, D. G., Duan, X., and Li, C. Y., *Microporous Mesoporous Mater*. **44–45**, 581 (2001).
10. Luan, Z., He, H., Zhou, W., Chen, C. F., and Klinowski, J., *J. Chem. Soc. Faraday Trans*. **91**, 2955 (1995).
11. Langhendries, G., De Vos, D. E., Baron, G. V., and Jacobs, P. A., *J. Catal*. **187**, 453 (1999).
12. Klein, S., and Maier, W. F., *Angew. Chem.* **108**, 2376 (1996).
13. Olson, D. H., Haag, W. O., and Lago, R. M., *J. Catal*. **61**, 390 (1980).
14. Zhang, F., Guo, X., Wang, X., Li, G., Zhou, J., Yu, J., and Li, C., *Catal. Lett.* **72**, 235 (2001).
15. Klaas, J., Schulz-Ekloff, G., and Jaeger, N. I., *J. Phys. Chem. B* **101**, 1305 (1997).
16. Blasco, T., Camlor, M. A., and Perez-Pariente, J., *J. Am. Chem. Soc.* **115**, 11806 (1993).
17. Jahn, S. L., Nascente, P. A. P., and Cardoso, D., *Zeolites* **19**, 416 (1997).